Environ Earth Sci (2013) 68:2301–2312
DOI 10.1007/s12665-012-1909-3

ORIGINAL ARTICLE

Particle-size effects on dissolved arsenic adsorption to an Australian laterite

Raul Mollehuara Canales · Huade Guan · Erick Bestland · John Hutson · Craig T. Simmons

Received: 15 July 2011 / Accepted: 11 August 2012 / Published online: 30 August 2012

Abstract In this study, arsenic adsorption to an Australian laterite has been examined for a particle-size range between 38 μm and 25 mm. The results show that particle size influences both kinetic and equilibrium characteristics of arsenic adsorption. The equilibrium adsorption capacity increases from around 100 mg kg^{-1} for laterite particles coarser than 4 mm, to around 160 mg kg^{-1} for laterite particles between 75 μm and 4 mm, and to over 200 mg kg^{-1} for laterite particles finer than 75 μm. The kinetic adsorption data can be fitted with the pseudo-second-order reaction model, in particular for finer particles where the film diffusion and/or surface reaction are important processes. The model-fitted rate constant remains steady for laterite particles coarser than 2 mm, increases moderately with particle size in the range between 75 μm and 2 mm, and increases dramatically for laterite particles finer than 75 μm. These arsenic adsorption behaviours can be explained by the relative importance of two particle-size-dependent processes: quick external-surface adsorption (more important for fine particles) and slow intraparticle adsorption (more important for coarse particles). Most of the external-surface adsorption completes in the first hour of the experiment. To apply the studied laterite for dissolved arsenic removal, it is recommended that fine particles, in particular finer than 75 μm, should be used if the contact time is the limitation, and that coarse particles, in particular 2–4 mm, should be used if sufficient contact time is available.

Keywords Natural laterite · Arsenic removal · Adsorption · Particle-size effect · Intraparticle diffusion · Kangaroo Island

R. Mollehuara Canales · H. Guan (✉) · E. Bestland · J. Hutson · C. T. Simmons
School of the Environment, Flinders University, Sturt Road, Bedford Park, Adelaide, SA 5042, Australia
e-mail: huade.guan@flinders.edu.au

H. Guan · C. T. Simmons
National Centre for Groundwater Research and Training, Flinders University, Sturt Road, Bedford Park, Adelaide, SA 5042, Australia

Introduction

Arsenic is considered as one of the most hazardous chemical in the world (Mondal et al. 2006). Exposure to arsenic can cause serious health problems, including both acute and chronic effects (NRC 2001). For example, a lifetime exposure to drinking water of 50 μg l^{-1} arsenic increases cancer risk by 100 times in comparison to drinking water of 0.5 μg l^{-1} arsenic (NAS 1999). In 1993, World Health Organization (WHO) has recommended a maximum contaminant level of 10 μg l^{-1} for arsenic in drinking water (WHO 1993), which has been accepted by many countries. Arsenic exists in the environment in various forms (Smedley and Kinniburgh 2002). In aqueous environments, the two most common forms of inorganic arsenic are arsenate [As(V)] in the oxic condition, and arsenite [As(III)] in the anoxic condition (Oremland and Stolz 2003). As(III) is more toxic and more mobile in water than As(V) (Mondal et al. 2006). It is found predominantly in contaminated groundwater and more difficult to remove in comparison to As(V).

Methods, based on either physico-chemical techniques, or biological techniques, can be used for arsenic removal from contaminated water (Mondal et al. 2006). Among these, arsenic removal techniques using reactive adsorbents are considered cost-effective and technically simple. These

adsorption techniques can be applied in fluidized bed systems, fixed-bed systems (Inglezakis and Poulopoulos 2006), or in situ permeable reactive barriers (Blowes et al. 2000; Gibert et al. 2010). Various adsorbents, including iron oxide and its coated media (Dixit and Hering 2003; Genc-Fuhrman et al. 2004; Guo et al. 2008; Jonsson and Sherman 2008; Raven et al. 1998), granular titanium dioxide, natural iron ores, zero-valent iron, and activated alumina, have been used to remove arsenic from water (Mohan and Pittman 2007; Mondal et al. 2006). In this category, naturally occurring, low-cost laterite has recently been tested for arsenic removal from water (Jahan et al. 2011; Maiti et al. 2007, 2008; Maji et al. 2007, 2008; Partey et al. 2006).

Current knowledge about the processes influencing adsorption is well summarized in (Plazinski et al. 2009). These processes include: (1) transport of solute in the bulk solution; (2) solute diffusion across the liquid film between the bulk solution and the adsorbent particle, hereafter referred to as film diffusion; (3) solute diffusion inside the adsorbent particles to the internal pore surfaces, hereafter referred to as intraparticle diffusion; and (4) adsorption and desorption of solute to and from the adsorbent surfaces, hereafter referred to as surface reaction.

Adsorbent particle size has effects on these adsorption-controlling processes. Particles of a smaller size expose more adsorption sites on the external surface, on which the adsorption of contaminant molecules (or ions) occurs. The film diffusion rate and the surface reaction rate are important (probably predominant) controlling factors. Particles of a larger size have more adsorption sites in the internal pores. Adsorption to these sites is controlled by both the intraparticle diffusion rate and the surface reaction rate. The adsorbent particle size also influences the adsorption capacity because fine particles tend to have more adsorption surface area per unit mass. The above discussion assumes no limitation on moving the contaminant molecules (or ions) from bulk solution to the liquid and adsorbent solid interface. In reality, if the adsorbent particle sizes are too fine in the fixed-bed or in situ permeable barrier systems, low permeability of the system may either restrict water flow through the system, and consequently limit contaminant movement from the bulk water to adsorbent solid and liquid interface, or otherwise request high-energy input to force water flow through the system. Thus, from this perspective, coarse particles are preferred for the fixed-bed and in situ permeable reactive barrier systems because they provide high hydraulic conductivity (Schulze-Makuch et al. 2003).

Laterite can be easily broken into various particle sizes. Knowledge of how particle size impacts its adsorption performance is useful to design laterite-based fixed-bed or in situ permeable reactive barrier systems. Particle sizes used in previous laterite adsorption experiments ranged from finer than 63 μm (Partey et al. 2006), 53–212 μm (Jahan et al. 2011), 0.36–0.55 mm (Maiti et al. 2007), to 0.25–0.65 mm (Maiti et al. 2009), with the adsorbent particle size effect being examined for 0.25–0.65 mm (Maiti et al. 2009). Maiti et al. (2009) investigated the kinetics of arsenic absorption to natural laterite for three particle sizes (0.25, 0.38, and 0.65 mm), and found that the decay rate of bulk arsenic concentration is faster for finer laterite particles, which is attributed to a larger specific surface area of the finer particles. In this study, natural laterite samples over a larger range of particle size distribution (38 μm–25 mm) are examined. The objectives are to investigate the effects of particle size on laterite removal of dissolved arsenic from water, and to understand the mechanisms of the size-dependent kinetic adsorption behaviours.

Materials and methods

Laterite adsorbent preparation and mineralogical testing

Laterite collected from Kangaroo Island (KI) of South Australia has been shown to be a good adsorbent for arsenic removal from water (Jahan et al. 2011), and has been selected for this study. The sample of KI laterite was obtained from a consolidated, iron-cemented, nodular (pisolithic) horizon that occurred extensively on the north-western portion of KI. This horizon has been utilized as road gravels due to its abundance and occurrence in or near the upper surface of the soil profile. The laterite is extensive on the dissected plateau of the western half of KI. The mineral composition of KI laterite was tested using X-ray diffraction (XRD). X-ray diffraction spectra were measured using Co X-rays ($\lambda = 1.7902$ Å) over the range of 5°–90° to determine the crystalline phases present. A 100-g sample was ground to finer than 100 μm, and analysed by XRD. And the isoelectric point (IEP, the water pH in which laterite particles of multiple mineral compositions show bulk zero surface charge) was tested using a colloidal dynamics AZR II electroacoustic spectrometer which measures the sound waves generated from the oscillation of charged particles in an alternating electric field. Both measurements were conducted at Ian Wark Research Institute, University of South Australia. Chemical composition of KI laterite was tested using inductively coupled plasma (ICP) by ACME Analytical Laboratories Ltd, Canada.

Laterite samples of different particle size distribution (PSD) were prepared mechanically. The aim was to produce different size ranges for the adsorption experiments. Each PSD sample was described quantitatively by sieve

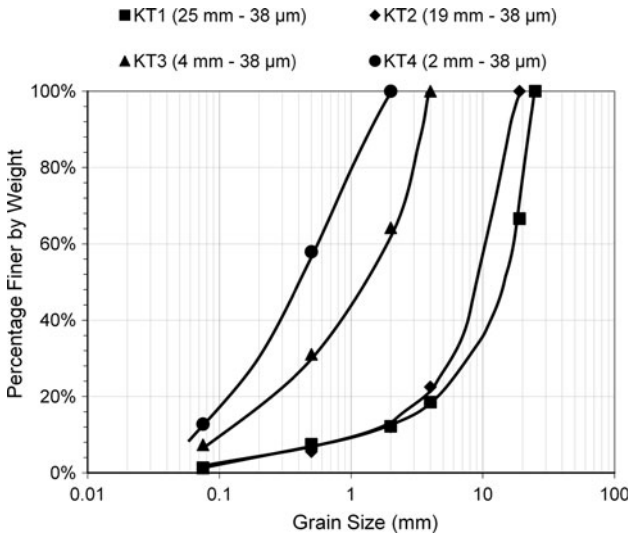

Fig. 1 Particle size distribution (PSD) of the four bulk laterite samples used in this study

analysis. A jaw crusher was applied on the laterite aggregate (total mass of 20 kg) to produce the first PSD sample (KT1, 38 μm–25 mm). A portion of KT1 sample was further processed in the jaw crusher by reducing the slit aperture (a long narrow opening between the jaws of the crusher where the sample passed through), resulted in the second PSD sample (KT2, 38 μm–19 mm). A portion of KT2 was used to obtain the third (KT3, 38 μm–4 mm) and fourth (KT4, 38 μm–2 mm) PSD samples. Sample KT3 was obtained from a disc grinder for 5 s, and KT4 was prepared using a ring grinder for 15 s. Each of these samples (KT1, KT2, KT3, and KT4) was sieved and classified following the engineering classification of the American Society for Testing and Materials (ASTM Standard D2488) (Fetter 1988): coarse gravel (19–25 mm), fine gravel (4–19 mm), coarse sand (2–4 mm), medium sand (0.5–2 mm), fine sand (75 μm–0.5 mm), and silt (38–75 μm). Loosely bound particles were insignificant and separated completely during the sieving process. Based on the sieve analysis results, the particle size distributions are plotted in Fig. 1. To examine whether mineral composition varies with the particle size, KT1 and its size fraction samples of specific size intervals were examined using X-Ray diffraction (XRD) techniques.

Arsenic solution and testing

The arsenic (III) stock solution of a concentration of 1,000 mg l^{-1} (As) was prepared using dehydrated sodium arsenite ($NaAsO_2$) and ultrapure (MilliQ) water (18 MΩ cm^{-1}), and stored in an amber glass bottle. All samples of 50 mg l^{-1} concentration used in batch experiments were prepared from this stock solution. The arsenic concentration in the solution was measured using an atomic absorption spectrophotometer (Model: GBC 933 plus, Scientific Equipment Pty. Ltd.), with a detection limit of 0.4 mg l^{-1}.

Arsenic adsorption experiments

Arsenic removal batch experiments were done for all four laterite bulk PSD samples (KT1, KT2, KT3, and KT4) and the sub-samples of different size intervals derived from the four bulk samples. Specific size intervals (hereafter referred to as size fraction samples) were sieved from each of the four bulk samples. The size intervals were 19–25 mm, 4–19 mm, 2–4 mm, 0.5–2 mm, 75–500 μm, and 38–75 μm. Due to that different mechanical forces were applied to obtain the four bulk samples, the particle size distribution of subdivision samples of the same size interval varies with the source bulk samples. For example, a size fraction sample of 0.5–2 mm derived from KT4 should have more fine particles than the one derived from KT1.

For each batch, 10 g of laterite sample was mixed with 50 ml (dose, 200 g l^{-1}) arsenic solution with a concentration of 50 mg l^{-1}, in a 100-ml conical flask. The experiments were carried out at room temperature (21–24 °C). The flask was sealed with laboratory parafilm during the experiment, and placed on a platform rocker (Bio-Line, Edwards Instrument Company, Australia). The rocker speed was set at 20 cycles per minute, to mimic low hydraulic agitation in fixed-bed and permeable barrier systems. To avoid the influence of sampling for arsenic concentration testing on the subsequent arsenic adsorption, for each batch, a set of nine flasks containing identical mass of laterite and arsenic solution were used. Water samples with dissolved arsenic were tested at 10, 30, 60, 120, 240, 360, 480, 1440, and 2880 min. The solution pH and reduction potential (Eh) were measured using a pH-mV-Temp meter (Model WP-80, provided by TPS Pty Ltd, Australia) for the respective flask at these time steps. A control flask containing 50 ml ultrapure water and 10 g corresponding laterite sample was placed together with the batch, with pH and Eh being monitored at the end of the batch experiment.

Kinetic adsorption modelling

Kinetic adsorption data of laterite samples of various sizes were examined with the pseudo-first-order and pseudo-second-order kinetic adsorption models. These two models were found to well approximate the kinetic behaviours of the adsorption processes (Plazinski et al. 2009).

The pseudo-first-order model is formulated as

$$\frac{dq_t}{dt} = k_1(q_e - q_t) \quad (1)$$

where q_t and q_e are the arsenic concentration of the adsorption phase (mg kg^{-1}) at time t and at the equilibrium

condition, respectively, k_1 is the pseudo-first-order adsorption rate constant (min^{-1}). Equation (1) can be integrated from time zero ($q_0 = 0$) to time t, resulted in

$$\log(q_e - q_t) = \log(q_e) - \frac{k_1}{2.303}t \quad (2)$$

With q_t measured at different time steps during the experiments between the initial condition and the equilibrium, Eq. (2) can be solved for q_e and k_1 using the least-squared error method to make the left-hand side and right-hand side as close as possible. This fitting method may sometimes lead to an unrealistic q_e (Plazinski et al. 2009). If this happened, q_e was confined to within 10 % of the maximum observed q_t to find the best solution.The pseudo-second order adsorption model is shown as

$$\frac{dq_t}{dt} = k_2(q_e - q_t)^2 \quad (3)$$

where k_2 is the pseudo-second-order reaction rate constant [$(mg/kg)^{-1}min^{-1}$], other symbols were described previously. The integral form of Eq. (3) is

$$\frac{t}{q_t} = \frac{1}{k_2 q_e^2} + \frac{1}{q_e}t \quad (4)$$

In comparison to the pseudo-first-order model, the pseudo-second-order equation infers q_e from the data-fitting result.

To understand the particle-size effects on arsenic adsorption to laterite particles, it is important to recognize the relative importance of the film diffusion and surface reaction rates and the intraparticle diffusion rate. Generally, at the beginning of the experiments, arsenic adsorption primarily occurs on the external surface of the laterite particles. At this stage, film diffusion and surface reaction are the limiting factors. When the external-surface adsorption sites have been mostly consumed, adsorption to the internal surface adsorption sites becomes important. At this point, intraparticle diffusion starts to play a more important role in controlling the adsorption processes. During this time, the amount of adsorbed solute is proportional to the square root of the operating time (Maiti et al. 2007; McKay et al. 1987; McKay and Poots 1980; Singh et al. 1988).

$$q_t = X_0 + K_p t^{0.5} \quad (5)$$

where K_p is the intraparticle diffusion rate constant, t is time measured from the beginning of the adsorption experiment. Eq. (5) applies after intraparticle diffusion becomes the dominant limiting factor for adsorption. This time point is referred to as t_p. X_0 is a fitting parameter, whose physical meaning is not clear. Nonetheless, the q_t value at time t_p (denoted as X_s) can be approximated as the adsorption that has occurred to the external surface before the intraparticle adsorption becomes dominant. After this time point, adsorption primarily happens to the internal surface, during which the intraparticle diffusion and subsequent surface reaction on the internal pore surfaces become important. The physical meaning of Eq. (5) was discussed in McKay et al. (1987) where K_p was found insensitive to the agitation speeds. This is supportive evidence that K_p is related to the intraparticle adsorption, rather than the external-surface adsorption which is dependent of the agitation speeds. Meanwhile, McKay et al. (1987) also found that K_p increased with a decrease of the adsorbent mass, or an increase of initial solute concentration. This is because with either fewer adsorbent particles or more solute molecules (ions), the external-surface adsorption becomes less important in comparison to the intraparticle adsorption. Similar phenomenon was observed in Maiti et al. (2007). Thus, Eq. (5) is useful to examine the relative importance of intraparticle adsorption. It is hereafter referred to as the intraparticle adsorption model. Particle size of the adsorbent can influence both X_s and t_p. Thus, Eq. (5), when fitted with the kinetic adsorption data, provides useful information of the particle-size effect on the adsorption mechanism (i.e., external-surface adsorption vs. intraparticle adsorption).

Results

Chemical and mineral composition of the laterite samples

The chemical composition of KT1 bulk sample is shown in Table 1. The most abundant compositions are Al_2O_3, SiO_2, and Fe_2O_3, followed by TiO_2. The mineral composition of KT1 bulk sample and its size fraction samples are summarized in Table 2. The most abundant mineral estimated from the XRD result, is gibbsite (~60 %), followed by quartz (10–20 %), goethite (~10 %), rutile (5–10 %), and hematite (<5 %). The order of mineral abundance is consistent with that of chemical abundance shown in Table 1. The slightly high gibbsite composition, in comparison with Al_2O_3 composition in Table 1, is possible due to that kaolinite, difficult to quantify in XRD, was interpreted as gibbsite. The high percent of quartz (50 %) in the 19–25 mm size fraction sample is most likely due to less representative sample being sent for XRD analysis. The weight-mean mineral composition calculated from the size fraction samples is comparable to the measured mineral composition of KT1 bulk sample. Some difference in quartz and gibbsite content between measured and calculated bulk KT1 laterite can be attributed to overestimation of quartz in the 19–25 mm size fraction sample. Mineral composition is similar between the size fraction samples, except for rutile, which tends to be more abundant in the

Table 1 Chemical composition (weight percentage) of KI laterite measured with ICP, with total carbon being tested by Leco analysis, at the ACME Laboratories

SiO_2	Al_2O_3	Fe_2O_3	MgO	CaO	Na_2O	K_2O	TiO_2	P_2O_5	MnO	Cr_2O_3	LOI	Sum	Total carbon
27.82	31.92	18.15	0.08	0.10	0.03	0.12	0.55	0.02	<0.01	0.03	21.00	99.82	0.41

Table 2 Measured and calculated (mass-weighted average) mineral compositions and surface electrostatic properties of the KT1 bulk and size fraction samples

Mineral species		Quartz	Gibbsite	Rutile	Hematite	Goethite	Calculated IEP[b]
Theoretical PZC[a]		2.2	9.5	4.1	7.8	8	
Laterite samples	% KT1	%	%	%	%	%	
19–25 mm	33.4	47.7	41.3	2.9	1.7	6.4	5.7
4–19 mm	48.1	13.1	68.4	5.7	2	10.8	8
2–4 mm	6.4	9.4	73.4	5.4	1.5	9.8	8.3
0.5–2 mm	4.7	14.1	62.9	6.3	3.6	13.1	7.9
75–500 μm	6.2	16.7	54.8	19.1	1.9	7.4	7.1
38–75 μm	1.3	19.3	58.7	7.1	4.1	10.8	7.5
Calculated KT1 bulk sample		24.8	58.5	5.6	2.0	9.2	7.2
Measured KT1 bulk sample		11.3	69.6	5.7	2.5	10.8	6.1

[a] Point of zero charge, the pH value at which the mineral particle shows zero surface charge in water

[b] Isoelectric point, the pH value at which a mixture of particles or a particle of multiple mineral compositions shows bulk zero surface charge in water

75–500 μm size fraction sample. The measured isoelectric point of KT1 bulk sample is 6.1. No IEP was measured for size fraction samples. It is calculated as the sum of weight-mean theoretical point of zero charge of the mineral components. The IEPs (calculated or measured) of all laterite samples lie roughly between pH 6 and 8.

The pH and Eh of arsenic adsorption batch experiments

All together, 22 arsenic adsorption batch experiments were conducted. Four were for the bulk laterite samples (KT1, KT2, KT3, and KT4), and 18 for the size fraction laterite samples (Table 3). The pH and Eh values during the batch experiments are summarized in Fig. 2. The pH of blank samples (water and laterite only) tend to have pH around 7 (Fig. 2a). For the batches of coarse laterite particles (e.g., KT1 and KT2, and size fraction samples with a particle size larger than 0.5 mm), the pH was around 9 at the beginning, and gradually decreased to 8–8.5 at the eighth hour of the experiment. The high initial pH is apparently due to arsenite solution (6).

$$NaAsO_2 + 2H_2O = H_3AsO_3 + OH^- + Na^+ \quad (6)$$

As shown in (7) (Maiti et al. 2007), the adsorption of arsenite does not influence water pH.

$$MOH_{(s)} + H_3AsO_{3(aq)} = MH_2AsO_3 + H_2O \quad (7)$$

where M represents Fe or Al. Thus, it is more likely some dissolution of laterite minerals slowly decreases water pH. For the batches of fine laterite samples, the pH immediately decreased to below 7, and then increased to between 7 and 8. The immediate pH drop to below 7 was probably due to quick dissolution of fine laterite particles. Since arsenite adsorption does not change water pH, the increase in pH during the experiment may indicate some arsenate adsorption.

$$MOH_{(s)} + H_2AsO_{4(aq)}{}^- = MH_2AsO_4 + OH^- \quad (8)$$

High Eh in the solution of fine laterite particles at the beginning of the experiment (Fig. 2b), tends to support the possibility of arsenite oxidation to arsenate. This suggests that some arsenite oxidation may have occurred in the experiment. This is consistent with other studies (Maiti et al. 2007). Thus, arsenic adsorption is used which lumps

Table 3 The pseudo-second-order kinetic model-fitted parameters for arsenic adsorption experiments of the size fraction samples derived from the four bulk PSD laterite samples

Laterite samples	q_e $mg(kg)^{-1}$	k_2 $(mg/kg)^{-1}\ h^{-1}$	Number of batches
19–25 mm	105	0.0031	1
4–19 mm	105	0.0025	2
2–4 mm	159	0.0024	3
0.5–2 mm	172	0.0048	4
75–500 μm	164	0.0096	4
38–75 μm	204	0.0906	4

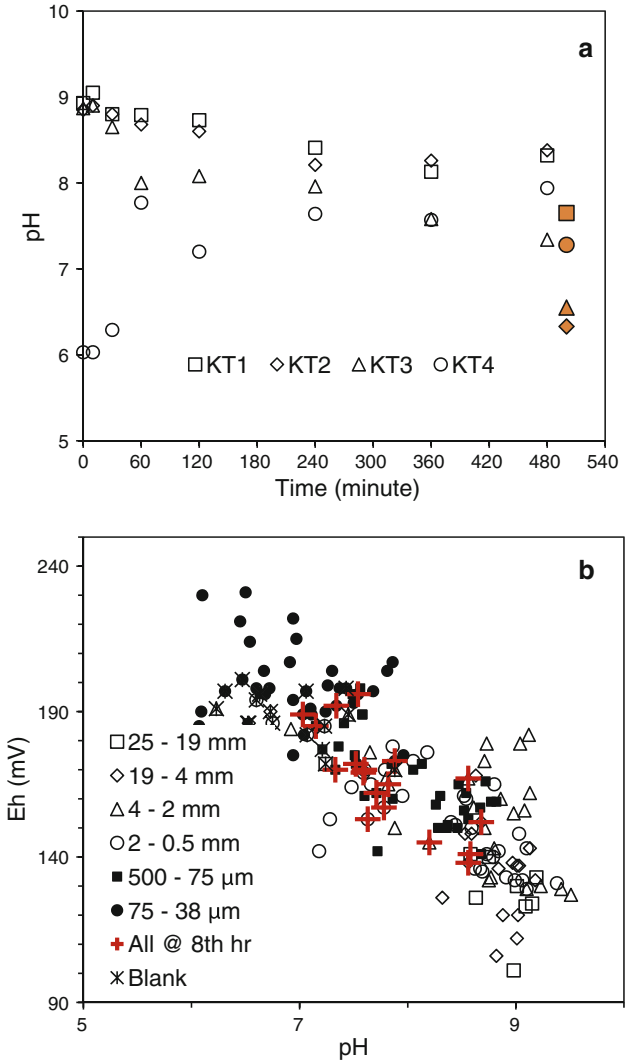

Fig. 2 **a** The pH evolution during the arsenic removal experiment using the four bulk laterite samples, with blank batches (water and laterite) shown in the *solid symbols*, and **b** the pH and Eh conditions during the first 8 h of the arsenic removal batch experiments using subdivision samples of specific size intervals obtained from each of the four bulk laterite samples. The conditions at the 8th hour of the experiments are shown in cross, and those of the blank flasks (water and laterite only) shown in *stars*

both arsenite and arsenate adsorptions in the following discussion.

Kinetic adsorption modelling

The results of arsenic adsorption for the size fraction samples are fitted with two kinetic adsorption models (Eqs. 2, 4) (Fig. 3). Overall, the pseudo-second order model fits the kinetic adsorption data better than the pseudo-first-order model, in particular for laterite of particle size finer than 4 mm. For laterite of particle size coarser than 4 mm, the pseudo-first-order model provides a good fit to the data, in one case even better than the pseudo-second-order model (Fig. 3a, b). Similar results are obtained for the adsorption experiments of the bulk laterite samples (Fig. 4): the pseudo-first-order model provides a good fit for KT1, KT2, and KT3 adsorption data, and the pseudo-second-order model for KT2, KT3, and KT4 data.

It is difficult to compare the fitted parameter values across the two models. Since the pseudo-second-order model provides fairly good fit for laterite adsorption results of all size fractions (although the pseudo-first order model performs slightly better for coarse particles), the fitted parameters are summarized for comparison between different particle size ranges (Table 3). It is found that particle size significantly influences both the adsorption capacity and adsorption rate constant. The adsorption capacity inferred from the fitted model is about 105 mg kg^{-1} for laterite of particle size coarser than 4 mm. It increases to 159–172 mg kg^{-1} for particle sizes between 0.075 and 4 mm, and to 204 mg kg^{-1} for laterite of particle sizes finer than 75 µm. In terms of the removal rate constant, the model-fitted value does not show much difference for particle sizes coarser than 2 mm, which is 0.0024–0.0031 $(mg/kg)^{-1}$ h^{-1}. For particle size of 0.5–2 mm, the rate constant doubles to a value about 0.0048 $(mg/kg)^{-1}$ h^{-1}. For the finer laterite particles of 0.075–0.5 mm, the adsorption rate constant further increases to about 0.0096 $(mg/kg)^{-1}$ h^{-1}. When the particle size reduces to below 75 µm, the adsorption rate constant jumps to 0.1 $(mg/kg)^{-1}$ h^{-1}. This indicates that the adsorption to laterite particles of sizes finer than 75 µm behaves significantly different from coarser laterite particles.

External-surface adsorption and intraparticle adsorption

To understand the particle-size effects on intraparticle diffusion processes, the adsorbed arsenic concentration is plotted with the square root of the adsorption time for two size fraction groups (Fig. 5a: 2–4 mm, and b: 38–75 µm). The linear pattern of the data for $t > t_p$ indicates that intraparticle diffusion process becomes predominant. From the start of this linear fitting, t_p is inferred. The adsorption phase concentration at t_p gives X_s. Similar plots were made for the batch experiment results with other size fraction samples. The adsorption data and inferred parameter values of selected size fraction laterite samples with four different ranges of particle sizes are summarized in Table 4.

These results show that intraparticle diffusion is more important for coarse adsorbent particles. For laterite particles coarser than 4 mm, the intraparticle diffusion starts to become predominant in controlling arsenic adsorption about 5 min after the experiment. For laterite particles finer than 4 mm, the control from film diffusion and/or surface reaction is more important. It takes about 1 h for the effect

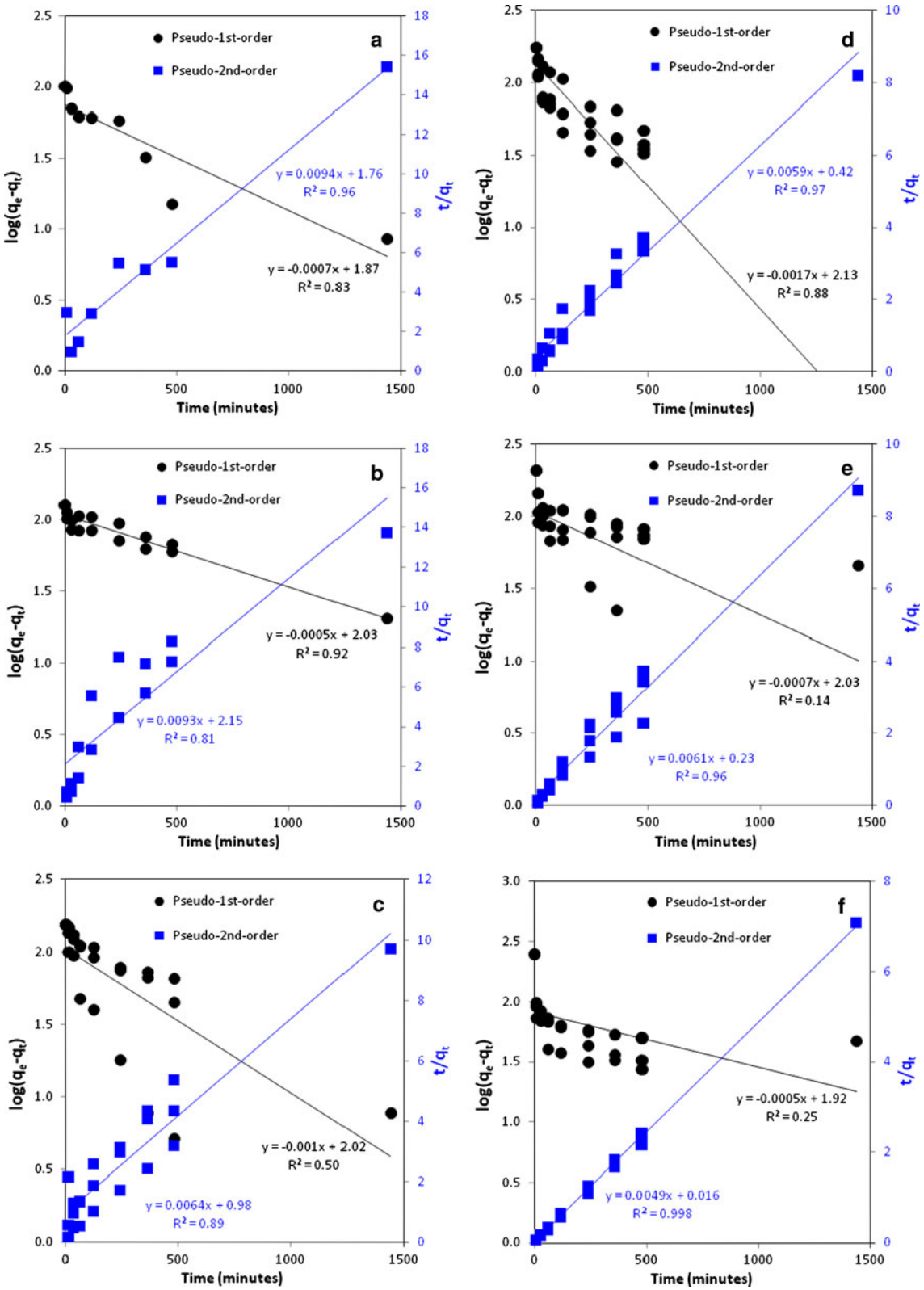

Fig. 3 Fitting results of the two kinetic adsorption models with the batch experiments of six size intervals: **a** (19–25 mm), **b** (4–19 mm), **c** (2–4 mm), **d** (0.5–2 mm), **e** (75–500 μm), and **f** (38–75 μm). The units are $mg(kg)^{-1}$ for q_t and q_e, and minutes for t

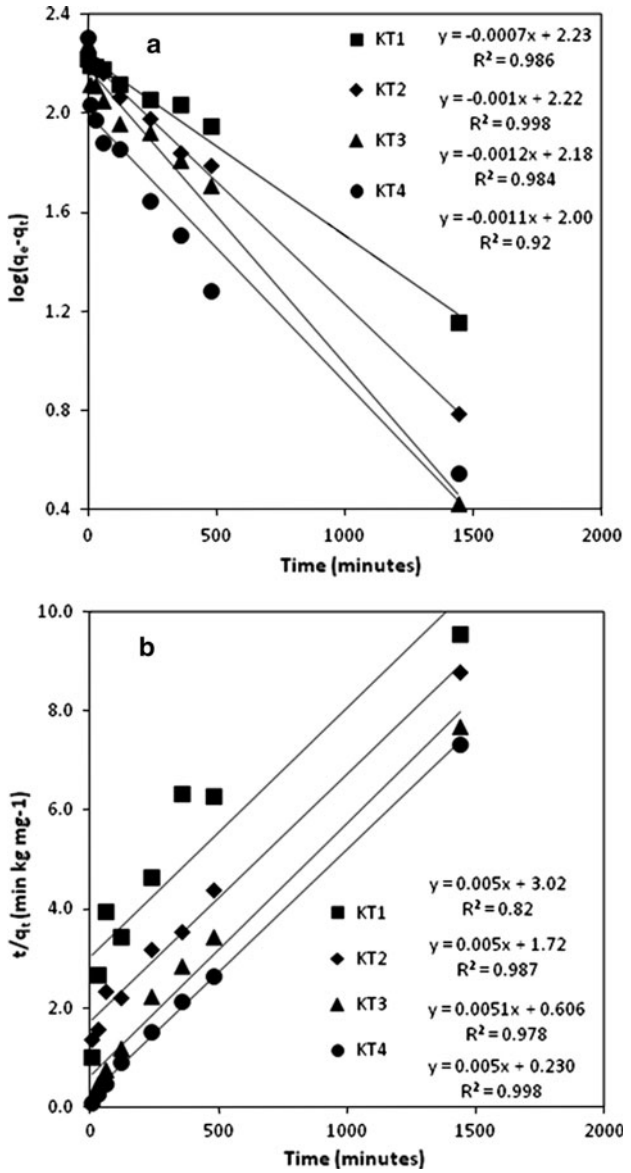

Fig. 4 Kinetic modelling results of arsenic adsorption to the bulk laterite samples of various PSD using: **a** the pseudo-first-order model, and **b** the pseudo-second-order model

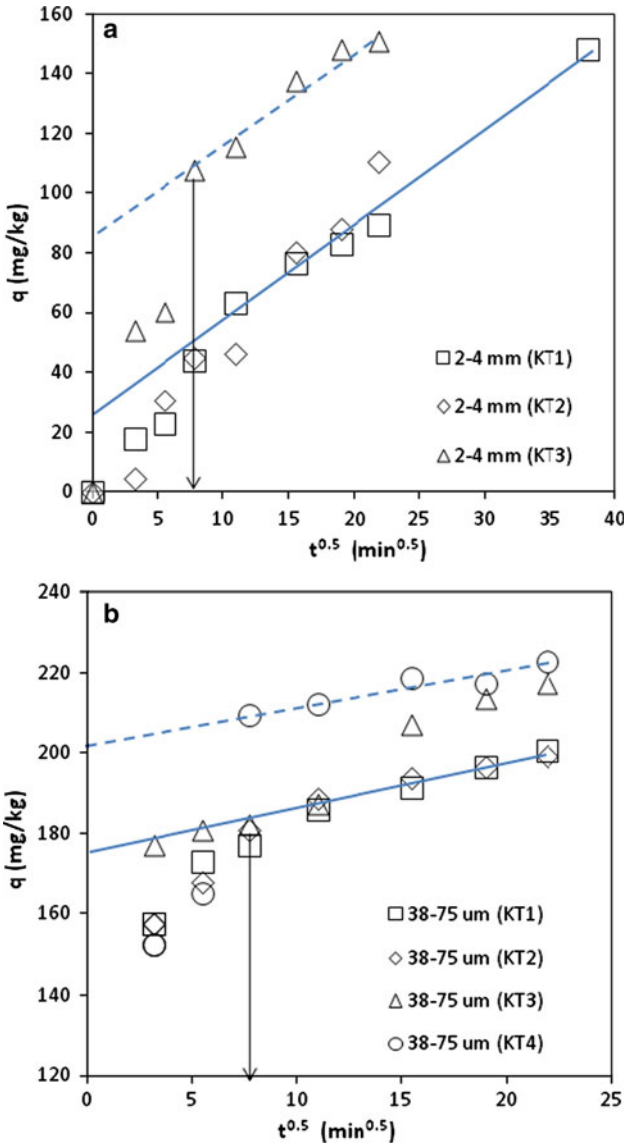

Fig. 5 Intraparticle mass transfer curve for arsenic adsorption on the size fraction samples of specific particle size intervals: 2–4 mm (**a**) and 38–75 μm (**b**)

of intraparticle diffusion to become predominant in controlling arsenic adsorption. In terms of intraparticle diffusion-controlled adsorption rate constant, it is around 3 (mg kg^{-1}) $min^{-0.5}$ for laterite particles coarser than 2 mm, and reduces to about 1 (mg kg^{-1}) $min^{-0.5}$ for laterite finer than 0.5 mm. This result indicates that pore structure is probably quite similar for laterite particles coarser than 2 mm, and is easier to facilitate arsenic diffusion into the intraparticle absorption sites. The pore structure in finer laterite samples becomes difficult for solute diffusion, and reduces the adsorption rate constant.

If arsenic absorption to the external surface is assumed negligible after t_p, the total arsenic adsorption on the external surface is estimated somewhere around X_s (Fig. 5). Relative contribution of the external-surface adsorption to the total arsenic adsorption is then calculated as (X_s/q_e), where q_e is given in Table 3. For size fraction samples of 4–19 and 19–24 mm, X_s is less than 20 mg kg^{-1} (Table 4). The contribution of external-surface adsorption is less than 20 %, which occurs in the first 5–10 min of the adsorption experiment. For size fraction samples of 2–4 mm, X_s is estimated to be about 40 mg kg^{-1} for samples derived from KT1 and KT2 bulk laterite samples, and about 90 mg kg^{-1} for samples derived from KT3 (Fig. 5a). The contribution of external-surface adsorption is calculated to be 25 % for KT1 and KT2 size fraction samples, and 55 % for KT3 size fraction

Table 4 Eq. (5) fitted parameter values showing the relative importance of the external surface adsorption and the intraparticle adsorption of selected size fraction samples

Laterite samples		Xs mg/kg	Kp $(mg/kg)^{-1}$ $min^{-0.5}$	tp hour
19-25 mm (KT1)		<20	3.1	0.1
4-19 mm	KT1			
	KT2			
2 - 4 mm	KT1	40	3.2	1
	KT2			
	KT3	90	3.2	1
0.5 -2 mm	KT1	90	1.9	1
	KT2			
	KT3			
	KT4	NA	NA	NA
38 - 75 μm	KT1	175	0.95	1
	KT2			
	KT3	NA	NA	NA
	KT4	205	0.95	1

Note: the results of 75-500 μm samples are difficult to be fitted with the intraparticle adsorption model, probably due to a relative high rutile concentration in this size fraction in comparison to others

sample. This is because KT3 (2–4 mm) size fraction sample has more abundant fine particles than the other two. The external-surface adsorption was nearly completed in the first hour of the experiment. For size fraction sample of 0.5–2 mm, X_s is estimated to be about 90 mg kg^{-1}, equivalent to 53 % of total equilibrium arsenic adsorption. For size fraction sample of 38–75 μm being derived from KT1 and KT2, X_s is estimated to be 175 mg kg^{-1}, equivalent to 87 % of the total equilibrium adsorption. For the KT4 (38–75 μm) size fraction sample, X_s is estimated to be 205 mg kg^{-1}, which is larger than q_e in Table 3. This is due to q_e being reported in Table 3 as lumped-estimation for the size fraction (38–75 μm) samples derived from KT1, KT2, KT3 and KT4. If a value of 220 mg kg^{-1} (Fig. 5b) is used as the adsorption capacity for KT4-derived size fraction sample, contribution of the external-surface adsorption accounts for 93 % of the adsorption capacity.

Arsenic adsorption to the bulk laterite samples

The results of arsenic adsorption to the bulk laterite samples are summarized in Fig. 6. Quicker and a greater quantity of adsorption occurs for the finer laterite particles. For KT4 bulk laterite, 50 % of adsorption capacity occurs in 30 min, while for KT1, it takes 8 h for arsenic adsorption to reach 50 % capacity. At the eighth hour of the experiments, arsenic adsorption to KT1, KT2, and KT3 is 1/3, 2/3 and 5/6 of that to KT4, respectively. After 24 h, the

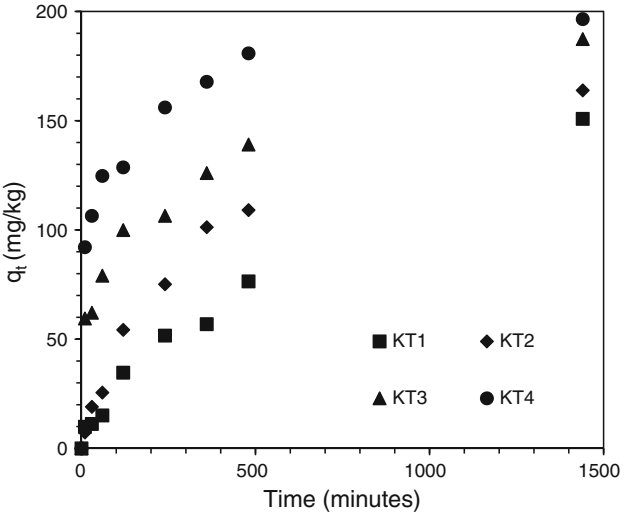

Fig. 6 Accumulated arsenic adsorption versus time for the bulk laterite samples of different particle size distribution, with an initial arsenic concentration of 50 mg l^{-1}

difference between the four bulk laterite samples becomes smaller (within 25 %).

The contribution of each size interval to the total arsenic adsorption in the bulk laterite sample is calculated from the size fraction results and the particle size distribution of the bulk laterite, as shown in Fig. 7. The results indicate that for KT1 and KT2, laterite particles finer than 2 mm contribute more arsenic adsorption, relative to their weight percentage in KT1 and KT2. For KT3 and KT4, laterite particles finer than 75 μm contributes a larger portion of arsenic adsorption relative to their weight percentage, while the arsenic adsorption to particle size between 75 μm and 2 mm does not show much difference.

Discussion

The results of kinetic arsenic adsorption experiments for laterite samples of various particle size distribution reveal that film diffusion, surface reaction, and intraparticle diffusion play roles in controlling arsenic adsorption, with relative contribution depending on adsorbent particle sizes. Film diffusion and surface reaction, associated with arsenic adsorption to the external surface, is the major controlling factor at the beginning of the experiment. Intraparticle diffusion becomes predominant in about 1 h of the experiment, suggesting that most of the external-surface adsorption is completed in the first hour of the experiment (Table 4). The time length for external-surface adsorption is not size dependent, except for the particle size coarser than 4 mm. It takes less than 10 min to complete most of the external-surface adsorption for laterite particles coarser than 4 mm.

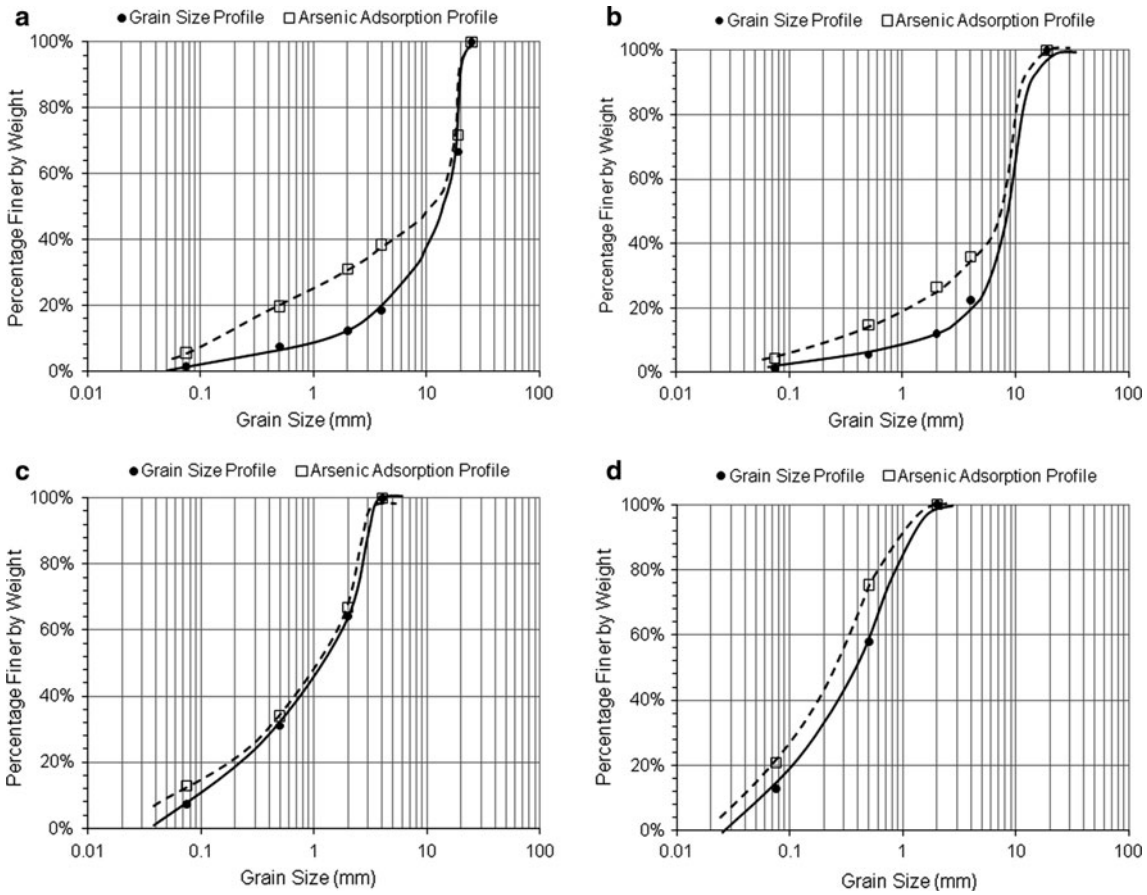

Fig. 7 Cumulative contribution to arsenic adsorption at each particle size interval in comparison to the particle size distribution of the four bulk laterite samples: KT1 (**a**), KT2 (**b**), KT3 (**c**) and KT4 (**d**)

The adsorption data of coarse laterite samples (e.g., KT1, 4–19 mm size fraction samples) are fitted better with the pseudo-first-order kinetic adsorption model, while those of fine-grained laterite samples (KT4 and size fraction samples finer than 4 mm) fit better with the pseudo-second-order kinetic adsorption model (Figs. 3, 4). This suggests that the pseudo-first-order kinetic model is more appropriate to represent the intraparticle adsorption, and the pseudo-second-order kinetic model is appropriate for the external-surface adsorption.

The relative contribution of external-surface adsorption and intraparticle adsorption varies with particle sizes of the laterite samples. The portion of total adsorption attributed to the external-surface adsorption increases from below 20 % for laterite coarser than 4 mm, to above 90 % for laterite particles finer than 75 μm. The overall arsenic adsorption rate is larger for the finer laterite samples, mainly owing to that external-surface adsorption contributes to a larger portion of total adsorption to the finer particles.

The size fraction laterite samples coarser than 4 mm have a similar adsorption capacity (Table 3) and intraparticle adsorption rate constant (Table 4). For this range of coarse laterite particles, the intraparticle adsorption contributes to the majority of arsenic removal from water. It thus takes a longer time (much longer than 1 h) to reach adsorption capacity. Little difference in adsorption capacity is observed for size fraction samples between 75 μm and 4 mm. For this particle range, the pseudo-second-order adsorption rate constant moderately increases with a decrease in particle size. For laterite finer than 75 μm, both the adsorption capacity and the pseudo-second-order rate constant abruptly increase, indicating that at this size level, more reactive adsorption sites may be exposed than the coarser particles. Intraparticle adsorption still exists for laterite particles finer than 75 μm (Fig. 5b), although its contribution to the total adsorption is small (~10 %). In this context, adsorbents with particle sizes at nanometer scales have recently been found improving arsenic removal from water, due to the different physical and chemical properties from that of regular sizes are exposed at the nanoparticle surfaces (Yean et al. 2005).

Among the batch experiments with various size fraction samples, the results for the 75–500 μm size fraction

samples do not fit well with the intraparticle adsorption model. This size fraction sample of laterite has significantly more rutile (Table 2). Rutile has been shown to be effective in converting As(III) to As(V) (Partey et al. 2006). It is possible that, for the batches with 75–500 μm size fraction laterite samples, more As(V) was formed, which lead to different adsorption behaviour than other batches. For example, under the experimental condition, As(V) exists as anions in the solution, while As(III) are neutral molecules. Electrostatic interactions can influence the adsorption processes of As(V), but not that of As(III).

Conclusions

In this study, arsenic adsorption batch experiments were performed for Kangaroo Island laterite of various particle size distributions, over a range between 38 μm and 25 mm. The results show that particle size influences both kinetic and equilibrium characteristics of arsenic adsorptions. The equilibrium adsorption capacity increases from around 100 mg kg^{-1} for laterite particles coarser than 4 mm, to around 160 mg kg^{-1} for laterite particles between 75 μm and 4 mm, and to over 200 mg kg^{-1} for laterite particles finer than 75 μm. The kinetic adsorption data can be fitted with the pseudo-second-order reaction model. The model inferred rate constants are similar for laterite particles coarser than 2 mm, moderately increase with particle size in the range between 75 μm and 2 mm, and abruptly increase for the laterite particles finer than 75 μm.

These arsenic adsorption behaviours are interpreted to be a result of size-dependent relative contributions of external-surface adsorption and intraparticle adsorption. The results from the intraparticle adsorption model suggest that both external-surface adsorption and intraparticle adsorption contribute to arsenic removal from water, but with relative contribution varying with laterite particle sizes. The adsorption capacity of particle size coarser than 4 mm is mainly owing to intraparticle adsorption (>80 % adsorption capacity), thus does not show much size-dependency. For laterite particles finer than 4 mm, the contribution from the external-surface adsorption increases, up to 70 % adsorption capacity for the particle size of 75–500 μm, and to over 90 % adsorption capacity for laterite of particle size finer than 75 μm.

Particle size of laterite samples has a large impact on the kinetic behaviour of arsenic adsorption. Finer particles speed the adsorption process presumably by providing greater surface area for quick external-surface adsorption. Most of the external-surface adsorption completes in the first hour of the experiment. With sufficient contact time, more intraparticle adsorption in the coarse particles reduces the difference in adsorption capacity between the laterite of different particle sizes. Thus, to apply the studied laterite for dissolved arsenic removal, it is recommended that fine particles, in particular finer than 75 μm, should be used if the contact time is the limitation, and that coarse particles, in particular 2–4 mm, should be used if sufficient contact time is available.

References

Blowes DW, Ptacek CJ, Benner SG, McRae CWT, Bennett TA, Puls RW (2000) Treatment of inorganic contaminants using permeable reactive barriers. J Contam Hydrol 45:123–137

Dixit S, Hering JG (2003) Comparison of arsenic(V) and arsenic(III) sorption onto iron oxide minerals: implications for arsenic mobility. Environ Sci Technol 37:4182–4189. doi:10.1021/es030309t

Fetter CW (1988) Applied hydrogeology, 4th edn. Prentice Hall, New Jersey

Genc-Fuhrman H, Tjell JC, McConchie D (2004) Adsorption of arsenic from water using activated neutralized red mud. Environ Sci Technol 38:2428–2434. doi:10.1021/es035207h

Gibert O, de Pablo J, Cortina JL, Ayora C (2010) In situ removal of arsenic from groundwater by using permeable reactive barriers of organic matter/limestone/zero-valent iron mixtures. Environ Geochem Health 32:373–378. doi:10.1007/s10653-010-9290-1

Guo HM, Stuben D, Bemer Z, Kramar U (2008) Adsorption of arsenic species from water using activated siderite-hematite column filters. J Hazard Mater 151:628–635. doi:10.1016/j.jhazmat.2007.06.035

Inglezakis VJ, Poulopoulos SG (2006) Adsorption, ion exchange and catalysis: design of operations and environmental applications, 1st edn. Elsevier, Amsterdam

Jahan N, Guan H, Bestland EA (2011) Arsenic remediation by Australian laterites. Environ Earth Sci 64:247–253. doi:10.1007/s12665-010-0844-4

Jonsson J, Sherman DM (2008) Sorption of As(III) and As(V) to siderite, green rust (fougerite) and magnetite: implications for arsenic release in anoxic groundwaters. Chem Geol 255:173–181. doi:10.1016/j.chemgeo.2008.06.036

Maiti A, DasGupta S, Basu JK, De S (2007) Adsorption of arsenite using natural laterite as adsorbent. Sep Purif Technol 55:350–359. doi:10.1016/j.seppur.2007.01.003

Maiti A, DasGupta S, Basu JK, De S (2008) Batch and column study: adsorption of arsenate using untreated laterite as adsorbent. Ind Eng Chem Res 47:1620–1629. doi:10.1021/ie070908z

Maiti A, Sharma H, Basu JK, De S (2009) Modeling of arsenic adsorption kinetics of synthetic and contaminated groundwater on natural laterite. J Hazard Mater 172:928–934. doi:10.1016/j.jhazmat.2009.07.140

Maji SK, Pal A, Pal T (2007) Arsenic removal from aqueous solutions by adsorption on laterite soil. J Environ Sci Health Part A-Toxic/Hazard Subst Environ Eng 42:453–462

Maji SK, Pal A, Pal T (2008) Arsenic removal from real-life groundwater by adsorption on laterite soil. J Hazard Mater 151:811–820. doi:10.1016/j.jhazmat.2007.06.060

McKay G, Poots VJP (1980) Kinetics and diffusion-processes in color removal from effluent using wood as an adsorbent. J Chem Technol Biotechnol 30:279–292

McKay G, Otterburn MS, Aga JA (1987) Intraparticle diffusion process occurring during adsorption of dyestuffs. Water Air Soil Pollut 36:381–390. doi:10.1007/bf00229680

Mohan D, Pittman CU (2007) Arsenic removal from water/wastewater using adsorbents—a critical review. J Hazard Mater 142:1–53. doi:10.1016/j.jhazmat.2007.01.006

Mondal P, Majumder CB, Mohanty B (2006) Laboratory based approaches for arsenic remediation from contaminated water: recent developments. J Hazard Mater 137:464–479. doi:10.1016/j.jhazmat.2006.02.023

NAS (National Academy of Science) (1999) Arsenic in drinking water, National Academy Press, Washington, DC

NRC (National Research Council) (2001) Arsenic in drinking water: 2001 update. The National Academies Press, Washington, DC

Oremland RS, Stolz JF (2003) The ecology of arsenic. Science 300:939–944

Partey F, Norman D, Ndur S, Siegel M (2006) Mechanism of arsenic sorption onto laterite iron concretions from Prestea, Ghana. Geochim Cosmochim Acta 70:A474–A474

Plazinski W, Rudzinski W, Plazinska A (2009) Theoretical models of sorption kinetics including a surface reaction mechanism: a review. Adv Colloid Interfac Sci 152:2–13. doi:10.1016/j.cis.2009.07.009

Raven KP, Jain A, Loeppert RH (1998) Arsenite and arsenate adsorption on ferrihydrite: kinetics, equilibrium, and adsorption envelopes. Environ Sci Technol 32:344–349

Schulze-Makuch D, Bowman RS, Pillai SD, Guan H (2003) Field evaluation of the effectiveness of surfactant modified zeolite and iron-oxide-coated sand for removing viruses and bacteria from ground water. Ground Water Monit Rem 23:68–74

Singh DB, Prasad G, Rupainwar DC, Singh VN (1988) As(III) removal from aqueous-solution by adsorption. Water Air Soil Pollut 42:373–386

Smedley PL, Kinniburgh DG (2002) A review of the source, behaviour and distribution of arsenic in natural waters. Appl Geochem 17:517–568

WHO (World Health Organisation) (1993) Guidelines for drinking water quality, Geneva, p 41

Yean S, Cong L, Yavuz CT, Mayo JT, Yu WW, Kan AT, Colvin VL, Tomson MB (2005) Effect of magnetite particle size on adsorption and desorption of arsenite and arsenate. J Mater Res 20:3255–3264. doi:10.1557/jmr.2005.0403